SUPPLEMENTAL DATA

Supplementary Figure 1

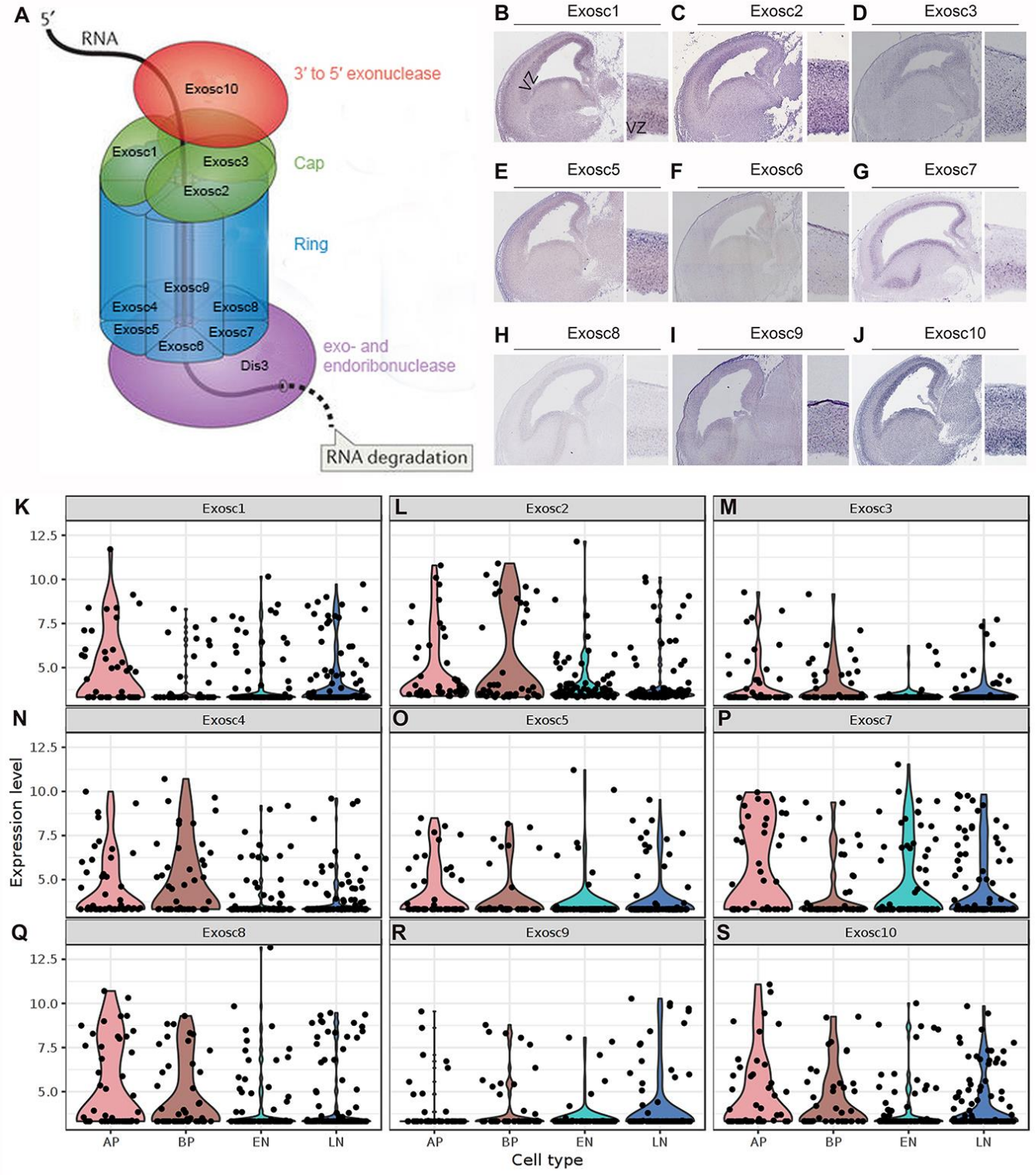

Figure S1. Expression of exosome complex subunits in the developing mouse brain.

(A) Model structure of the exosome complex with its components (Kilchert et al. 2016). (B–J) *In situ* hybridization of exosome complex components in sagittal sections of the E14.5 brains obtained from GenePaint database (Visel et al. 2004). Higher magnification of the cortex on right panels shows a high expression of exosome genes in the cortex, especially in the ventricular zone (VZ). (K–S) Expression of exosome subunits based on a published single-cell RNA-seq dataset of embryonic mouse cortex (Telley et al. 2016). The expression profiles of exosome subunits as violin plots was generated using the Seurat package of R (http://genebrowser.unige.ch/science2016/) (Macosko et al. 2015). AP: Apical progenitors/RGCs; BP: daughter basal progenitors/IPCs; EN: early-born neurons; LN: late-born neurons.

Supplementary Figure 2

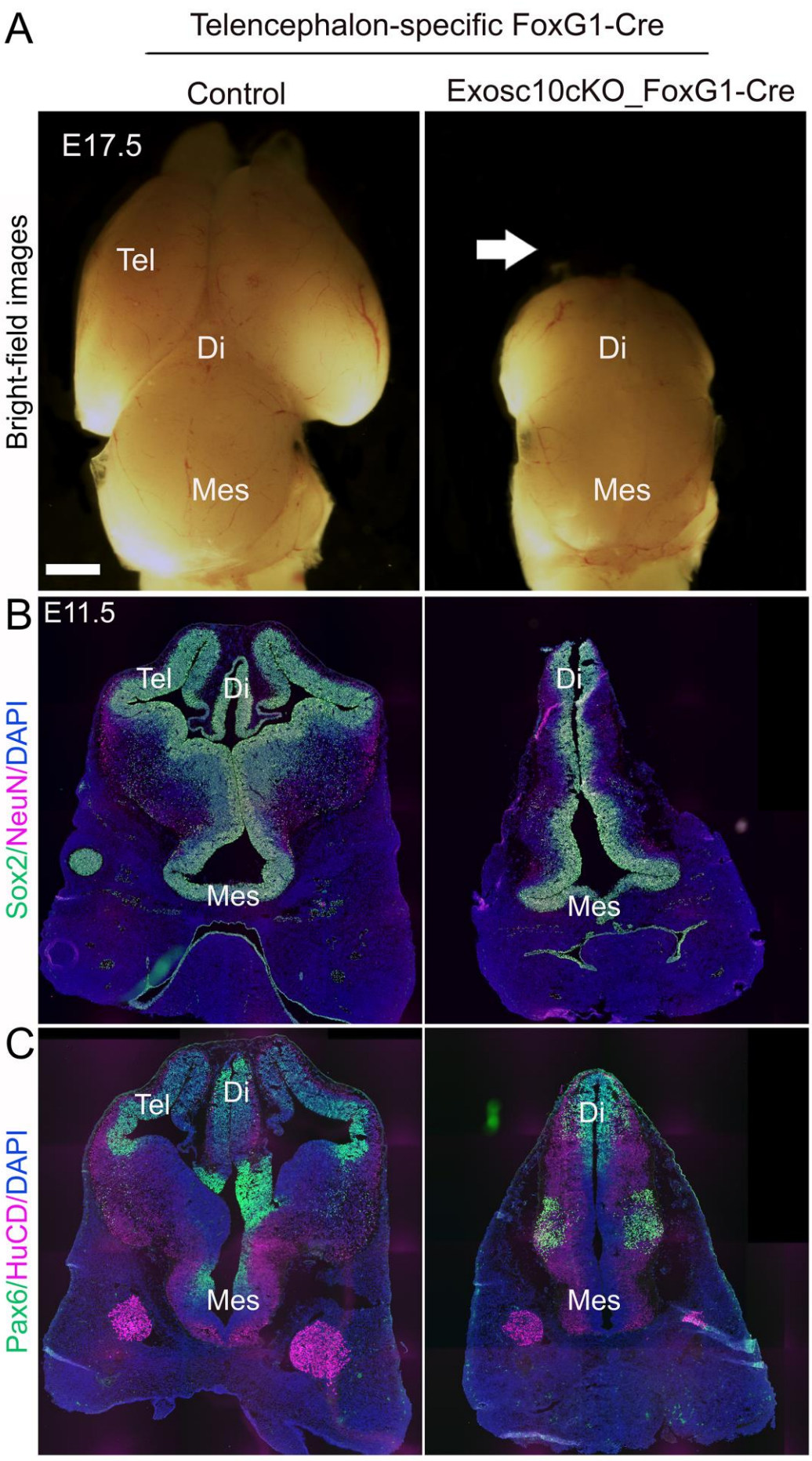

Figure S2. Expression of Exosc10 is required for specification of telencephalon.

(A) The forebrain-specific *dcKO_FoxG1*-Cre embryos have no telencephalon. (B, C) Representative images show IHC analyses with coronal sections of head from control and cKO_FoxG1-Cre embryos at E11.5 with antibodies against Sox2, NeuN (B) and Pax6, HuCD (C) that specifically label primordial NSC markers Sox2, Pax6, and immature neuronal markers NeuN, and HuCD respectively. IHC analyses revealed detectable Sox2+, Pax6+ NSCs and HuCD+, NeuN+ neurons in Diencephalon (Di) and in mesencephalon (Mes) in both control and cKO head, whereas these cell types were detected only in dorsolateral part (telencephalon, Tel) of control, but not that of cKO head. Abbreviations: Tel, telencephalon; Di, diencephalon; Mes, mesencephalon. Scale bars = 1 mm.

Supplementary Figure 3

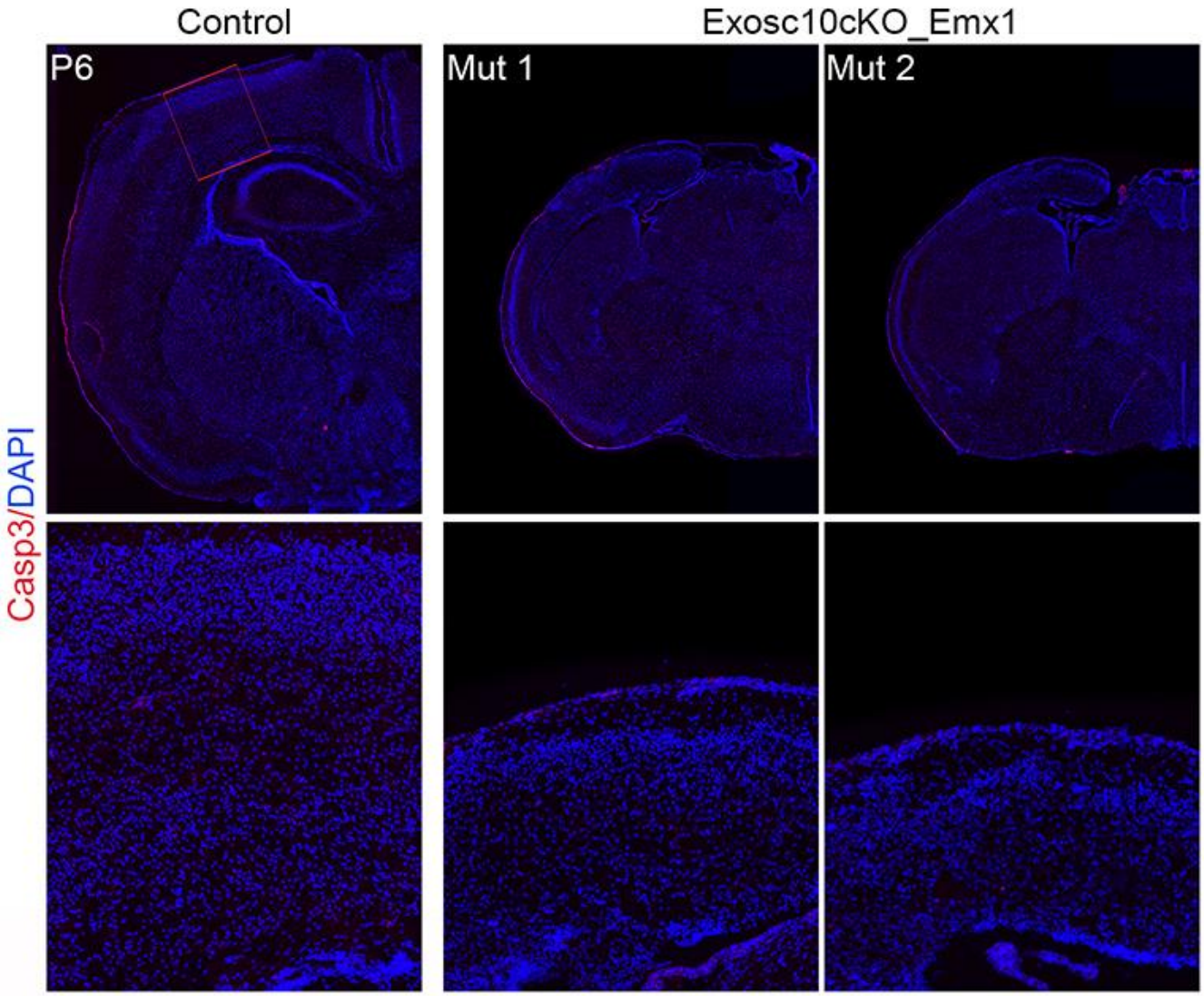

Figure S3. Exosc10 expression is not required for cell viability in postnatal cortex.

IHC analysis with antibody against Casp3 to detect cell death (counter staining with DAPI) indicated there was no obvious difference in number of Casp3+ apoptotic cells between control and Exosc10cKO cortices at P6.

Supplementary Figure 4

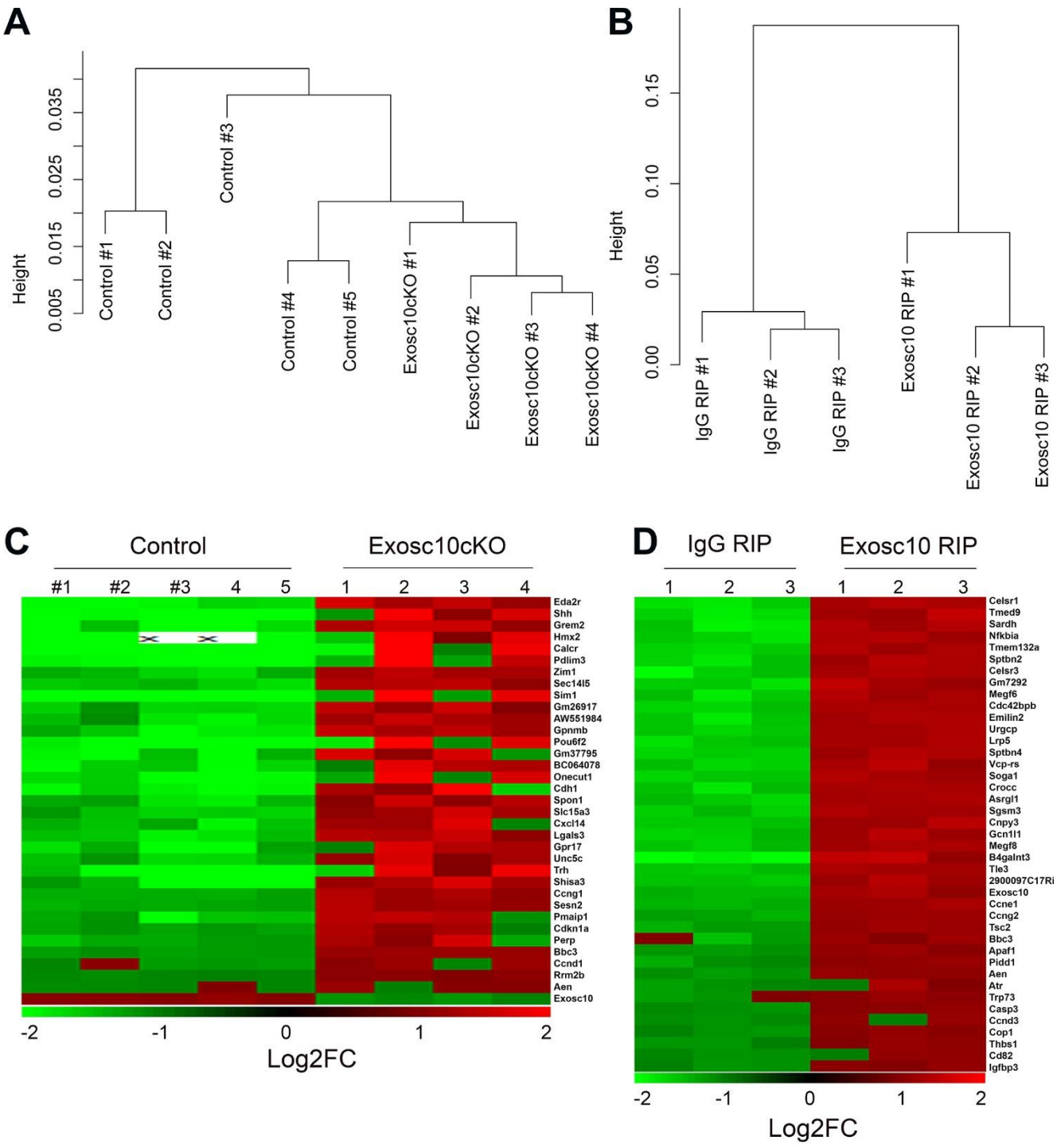

Figure S4. Cluster and Heatmap analyses of RNA-seq and RIP-seq samples.

(A, B) cluster dendrogram analysis of all RNA-seq (A, control, Exosc10cKO) and RIP-seq (B, IgG RIP, Exosc10 RIP) samples. The log2-nomalized values of all the genes were used for cluster analysis. (C, D) Heatmaps showing changes in gene expression (C) and transcript binding enrichment (D) revealed by RNA-seq (E12.5 Exosc10cKO cortex vs. control) and RIP-seq (E12.5 cortex, Exosc10 antibody vs IgG) analyses, respectively. Top 25 upregulated/enriched genes and genes involved in P53 apoptosis signalling were displayed. Additionally, Exosc10 was shown as a control.

Supplementary Figure 5

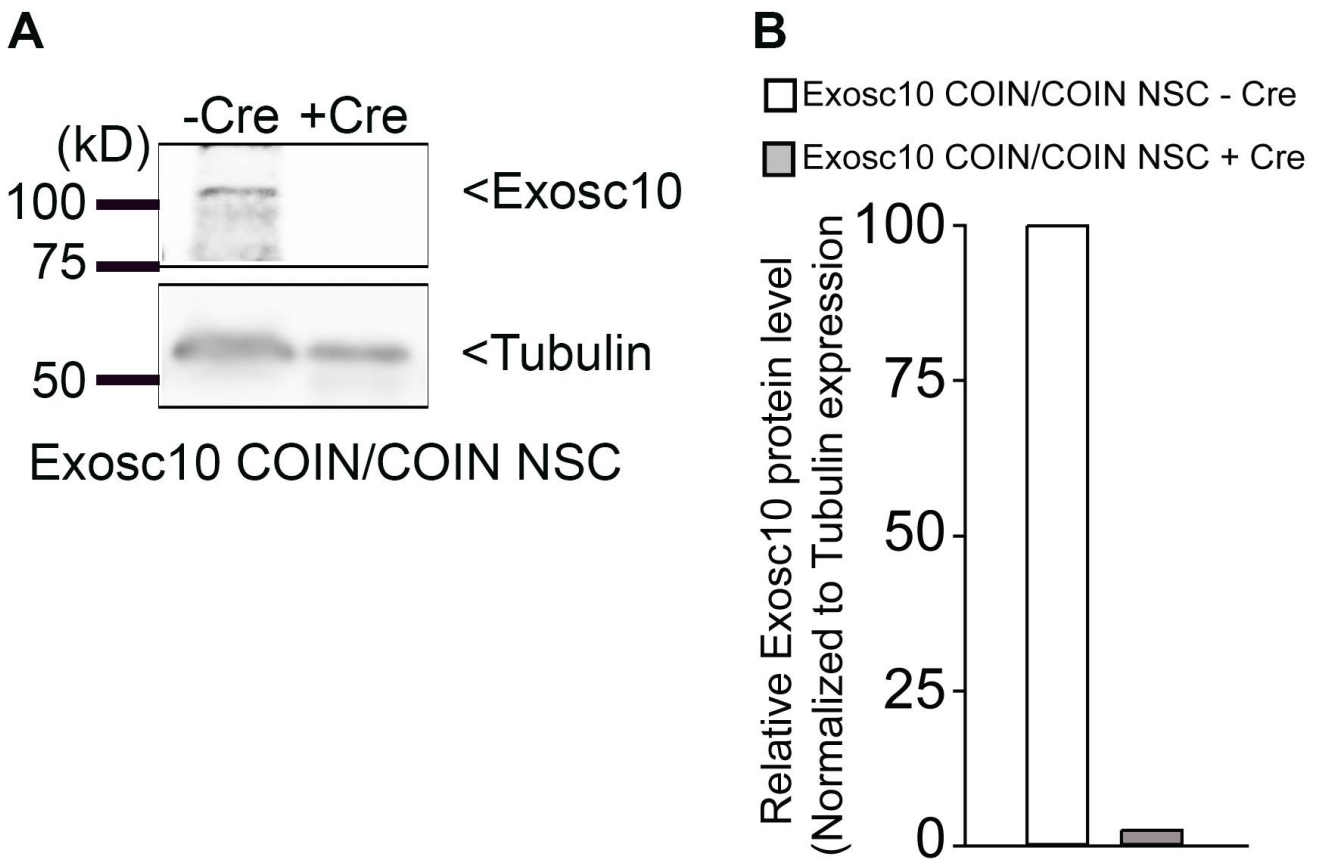

Figure S5. Knockout of Exosc10 using soluble Tat-Cre recombinase in Exosc10$^{COIN/COIN}$ NSCs and the effects of PFTα treatment on Bbc3 expression in the developing cortex.

(A) Western blot (WB) analysis of Exosc10 expression in Exosc10$^{COIN/COIN}$ NSCs without Cre (-Cre) as control and after 26h of treatment with soluble Tat-Cre recombinase (+Cre). Tubulin is shown as a loading control. (B) Quantification of the protein band densities (from A) relative to control (as 100%), which was normalized to tubulin.

Table S1. Genes regulated by Exosc10 in the Exosc10_*Emx1*-Cre cortex at E12.5

Click here to Download Table S1

Table S2. Gene Ontology Categories Significantly Enriched for upregulated genes in E12.5 Exosc10_*Emx1*-Cre cortex Compared with Controls in Expression Analyses

Click here to Download Table S2

Table S3. RIP-seq data for Exosc10 with E12.5 cortex

Click here to Download Table S3

Table S4. Gene Ontology Categories Significantly Enriched for transcripts bound by Exosc10 in RIP-Seq experiment

Click here to Download Table S4

Table S5. Overlap between upregulated genes in RNA-Seq of E12.5 Exosc10cKO cortex and transcripts bound by Exosc10 in RIP-Seq with E12.5 cortex.

Click here to Download Table S5

Table S6. Gene Ontology Categories Significantly Enriched for genes, in which their expression were upregulated in RNA-Seq of E12.5 Exosc10cKO cortex and their transcripts were bound by Exosc10 in RIP-Seq with E12.5 cortex

Click here to Download Table S6

Table S7. Statistical analyses

Click here to Download Table S7

Supplementary Materials and Methods

Antibodies

Polyclonal (pAb) and monoclonal (mAb) primary antibodies used in this study (working dilution; sources): Aen rabbit pAb (1:400; Bioss), Caspase-3 rabbit pAb (1:200; Cell Signaling), Ctip2 rat mAb (1:200; Abcam), Cux1 rabbit pAb (1:50; Santa Cruz), Exosc10 rabbit pAb (1:500 for WB; Proteintech), Exosc10 rabbit pAb (5µg for 100µl RIP-sample; Abcam), GFP chick pAb (1:400; Abcam), HuCD mouse mAb (1:20; Thermo Fisher Scientific), NeuN mouse mAb (1:200, Chemicon), Reelin mouse mAb (1:100), Satb2 mouse mAb (1:200; Abcam), Sox2 mouse mAb (1:100; Santa Cruz), Sox2 rat mAb (1:100; eBioscience), Sox5 rabbit pAb (1:100; Santa Cruz), Tbr1 rabbit pAb (1:300; Abcam), Tbr2 rabbit pAb (1:300; Chemicon), Tbr2 rat mAb (1:200; eBioscience), Tuj mouse mAb (1:500; Chemicon), Pax6 mouse mAb (1:100; Developmental Studies Hybridoma Bank). Secondary antibodies used were Alexa 488-, Alexa 568-, Alexa 594- and Alexa 647-conjugated IgG (various species, 1:400; Molecular Probes).

Relative quantification of cortical size

Relative quantification of cortical size was performed as described previously (Tuoc et al. 2013; Narayanan et al. 2018). Briefly, dorsal views of forebrains of mutant and control mice were photographed under a dissection microscope. Cortical anterior-posterior axis (AP), cortical surface and midline lengths from the digitized images were measured with Fiji software to make comparison between mutants and controls.

Immunohistochemistry (IHC)

IHC was performed as described previously (Tuoc et al. 2009). Briefly, Embryonic and postnatal brains were fixed in 4% paraformaldehyde, incubated in 25% sucrose in PBS-DEPC at 4°C overnight, embedded in Tissue-Tek O.C.T Compound (Sakura Finetek) on dry ice and cut in 8-16 µm coronal sections. After blocking with 5% goat or donkey normal serum, sections

were incubated overnight with primary antibody at 4°C and the signal was detected with a fluorescent secondary antibody (Alexa Fluor; 1:400; Invitrogen). Sections were later counterstained with Vectashield mounting medium containing 4'-6'-diamidino-2-phenylindole (DAPI) (Vector Laboratories) to label nuclei.

Quantitative RT-PCR (qPCR) and Western blot analyses

qRT-PCR and Western blot analyses were performed as described previously (Tuoc and Stoykova 2008b). Primers used for qPCR:

Aen

Forward: 5'-GGCCGGGTTTTCAGATCCTTA-3'
Reverse: 5'- GCTGAGCAGGTTTGGGACAT-3'

Bbc3

Forward: 5'-ACGACCTCAACGCGCAGTA-3'
Reverse: 5'-CTAGTTGGGCTCCATTTCTGG-3'

Atr

Forward: 5'-AGGACACTCCAAAGCACCACTG-3'
Reverse: 5'-GCAGCCCTGTTACTCTATTTCGG-3'

18S

Forward: 5'-CTTAGAGGGACAAGTGGCG-3'
Reverse: 5'-ACGCTGAGCCAGTCAGTGTA-3'

Cell counts and quantitative analysis of IHC signal intensity

IHC quantification was performed using anatomically matched coronal sections. Nucleus marker-positive cells were counted using the Cell Counter plugin of Fiji (Schindelin et al. 2012).

In most cases, cell counts of six matched sections were averaged (control/cKO). The number of lineage marker cells was quantified using the total marker-positive cells in a defined region (radial unit) alone, or by normalizing to the total number of DAPI+ (nucleus-stained) cells using the following equation: Normalized number = marker-positive cell number/DAPI+ cell number. For quantitative analyses of IHC signal intensity of cytoplasm-staining markers, fluorescent images of selected areas of the cortex were used. Color images were converted to gray scale and the fluorescent signal intensity values were measured using the Analyze/Measure function of Fiji software. The signal intensity from the background next to the tissue was subtracted from the measured intensity for normalization. The normalized intensities of cKO sections are displayed relative to normalized values from control experiments as a percentage. Statistical comparisons of histological data were performed using Student's t-test. All bar graphs are plotted as means ± SEM. All statistical tests are two-tailed, and P-values are considered to be significant for $p < 0.05$ ($*p < 0.05$, $**p < 0.01$, and $***p < 0.005$; NS, not significant).

SUPPLEMENTAL REFERENCES

Afgan E, Baker D, Batut B, van den Beek M, Bouvier D, Cech M, Chilton J, Clements D, Coraor N, Gruning BA et al. 2018. The Galaxy platform for accessible, reproducible and collaborative biomedical analyses: 2018 update. *Nucleic Acids Res* **46**: W537-W544.

Chen J, Bardes EE, Aronow BJ, Jegga AG. 2009. ToppGene Suite for gene list enrichment analysis and candidate gene prioritization. *Nucleic acids research* **37**: W305-311.

Huang da W, Sherman BT, Lempicki RA. 2009a. Bioinformatics enrichment tools: paths toward the comprehensive functional analysis of large gene lists. *Nucleic Acids Res* **37**: 1-13.

Kilchert C, Wittmann S, Vasiljeva L. 2016. The regulation and functions of the nuclear RNA exosome complex. *Nat Rev Mol Cell Biol* **17**: 227-239.

Love MI, Huber W, Anders S. 2014. Moderated estimation of fold change and dispersion for RNA-seq data with DESeq2. *Genome biology* **15**: 1.

Narayanan R, Pham L, Kerimoglu C, Watanabe T, Castro Hernandez R, Sokpor G, Ulmke PA, Kiszka KA, Tonchev AB, Rosenbusch J et al. 2018. Chromatin Remodeling BAF155 Subunit Regulates the Genesis of Basal Progenitors in Developing Cortex. *iScience* **4**: 109-126.

Oliveros J. 2007–2015. Venny. An interactive tool for comparing lists with Venn's diagrams.

Schindelin J, Arganda-Carreras I, Frise E, Kaynig V, Longair M, Pietzsch T, Preibisch S, Rueden C, Saalfeld S, Schmid B et al. 2012. Fiji: an open-source platform for biological-image analysis. *Nat Methods* **9**: 676-682.

Tuoc TC, Boretius S, Sansom SN, Pitulescu ME, Frahm J, Livesey FJ, Stoykova A. 2013. Chromatin Regulation by BAF170 Controls Cerebral Cortical Size and Thickness. *Developmental Cell* **25**: 256-269.

Tuoc TC, Radyushkin K, Tonchev AB, Pinon MC, Ashery-Padan R, Molnar Z, Davidoff MS, Stoykova A. 2009. Selective cortical layering abnormalities and behavioral deficits in cortex-specific Pax6 knock-out mice. *Journal of neuroscience* **29**: 8335-8349.

Tuoc TC, Stoykova A. 2008a. Trim11 modulates the function of neurogenic transcription factor Pax6 through ubiquitin-proteosome system. *Genes & development* **22**: 1972-1986.

Visel A, Thaller C, Eichele G. 2004. GenePaint.org: an atlas of gene expression patterns in the mouse embryo. *Nucleic Acids Res* **32**: D552-556.

Wang J, Duncan D, Shi Z, Zhang B. 2013. WEB-based GEne SeT AnaLysis Toolkit (WebGestalt): update 2013. *Nucleic Acids Res* **41**: W77-83.

Wang J, Vasaikar S, Shi Z, Greer M, Zhang B. 2017. WebGestalt 2017: a more comprehensive, powerful, flexible and interactive gene set enrichment analysis toolkit. *Nucleic Acids Res* **45**: W130-W137.

Zhang B, Kirov S, Snoddy J. 2005. WebGestalt: an integrated system for exploring gene sets in various biological contexts. *Nucleic Acids Res* **33**: W741-748.

Zhao C, Teng EM, Summers RG, Jr., Ming GL, Gage FH. 2006. Distinct morphological stages of dentate granule neuron maturation in the adult mouse hippocampus. *J Neurosci* **26**: 3-11.

Macosko EZ, Basu A, Satija R, Nemesh J, Shekhar K, Goldman M, Tirosh I, Bialas AR, Kamitaki N, Martersteck EM et al. 2015. Highly Parallel Genome-wide Expression Profiling of Individual Cells Using Nanoliter Droplets. *Cell* **161**: 1202-1214.

Telley L, Govindan S, Prados J, Stevant I, Nef S, Dermitzakis E, Dayer A, Jabaudon D. 2016. Sequential transcriptional waves direct the differentiation of newborn neurons in the mouse neocortex. *Science* **351**: 1443-1446.